Competing electronic orders in anisotropically strained $(Pr_{0.6}Ca_{0.4})_{1-x}(La_{0.6}Sr_{0.4})_xMnO_3$ thin films

J. S. Lee,[1,2,*] M. Nakamura,[3] D. Okuyama,[3] R. Kumai,[4] T. Arima,[5] M. Kawasaki,[3,6] and Y. Tokura[1,2,3]

[1]*Multiferroics Project, Exploratory Research for Advanced Technology (ERATO), Japan Science and Technology Agency (JST), c/o Department of Applied Physics, University of Tokyo, Tokyo 113-8656, Japan*

[2]*Department of Applied Physics and Quantum Phase Electronics Center (QPEC), University of Tokyo, Tokyo 113-8656, Japan*

[3]*Cross-Correlated Materials Research Group (CMRG) and Correlated Electron Research Group (CERG), ASI, RIKEN, Wako 351-0198, Japan*

[4]*Photonics Research Institute (PRI), National Institute of Advanced Industrial Science and Technology (AIST), Tsukuba 305-8562, Japan*

[5]*Institute of Multidisciplinary Research for Advanced Materials, Tohoku University, Sendai 980-8577, Japan*

[6]*WPI-Advanced Institute for Materials Research (AIMR), Tohoku University, Sendai 980-8577, Japan*

(Received 6 May 2010; published 31 August 2010)

We have explored the competing phases in the anisotropically strained manganese oxide with use of a composition-spread thin film where two contrastive ground states, i.e., ferromagnetic metal and charge/orbital-ordered insulator, are designed to compete with a continuous variation in the chemical composition. Taking advantage of a systematic inspection of the phase evolutions, we have confirmed that competing electronic orders could be realized in thin-film form. In particular, we found a possibly one-dimensional orbital-ordered insulating state near the metal-insulator phase boundary which can be disturbed by a relatively low magnetic field.

DOI: 10.1103/PhysRevB.82.052406 PACS number(s): 75.25.Dk, 75.47.Lx, 78.20.Ls, 78.30.Er

Competing orders and resultant phase instabilities in electronic states of a solid are of great importance for exploiting gigantic or sensitive responses against external stimuli. Realization of such functions has been made with use of thin films and/or junctions with the tuned phase competition and the stable homogeneity in electronic response over tens of nanometer to micron size. Transition-metal oxides with correlated electrons are promising hosts of such functionalities; e.g., insulator-metal or superconducting transition and magnetic transitions induced by electric/magnetic-field stimulation, light irradiation, heat, stress, etc. Compared to bulk materials, however, the phase competition in their thin-film form can be severely suppressed by the epitaxial strain from the substrate. For instance, when transition-metal oxides with simple cubic perovskite symmetry are grown on the (001) surface of the substrate as shown in Fig. 1(a), biaxial stress usually overwhelms other instabilities and makes the film inactive against additional stimuli. As an effort to minimize such strain effects, the films with a large thickness are grown to make the strain fully relaxed or vicinal substrates are sometimes used to release the accumulated elastic energy at the step edges.[1] The state-of-the-art thin-film technology provides us with another possibility to overcome this problem by exploiting the (011) orientation of the substrate as shown in Fig. 1(b).[2] In this case, only one axis is directly clamped to the substrate and hence the film gains more freedom so as to behave like a strain-free material. Recently, the charge/orbital-ordered state for some manganite thin films was realized by this method as in corresponding bulk materials,[2–4] which lowered the barrier in the thin-film technology of correlated-electron system toward its actual application targeting a wider range of bulk properties.

Here, we address the issue of phase competition in the thin-film system by investigating the anisotropically strained manganese oxide, $(Pr_{0.6}Ca_{0.4})_{1-y}(La_{0.6}Sr_{0.4})_yMnO_3$. $La_{0.6}Sr_{0.4}MnO_3$ and $Pr_{0.6}Ca_{0.4}MnO_3$ are the typical and contrastive systems, where the ferromagnetic metallic and charge/orbital-ordered insulating ground states are formed, respectively. Furthermore, a size mismatch of constituent ions is comparatively small between La and Sr as well as between Pr and Ca, which enables us to investigate competing long-range ordered phases depending on the composition with a minimal effect of the lattice disorder.[5,6]

The composition-spread film of $(Pr_{0.6}Ca_{0.4})_{1-y}(La_{0.6}Sr_{0.4})_yMnO_3$ was deposited on a (011) surface of the $(LaAlO_3)_{0.3}$-$(SrAl_{0.5}Ta_{0.5}O_3)_{0.7}$ substrate by pulsed laser deposition at 820 °C in an oxygen pressure of 5 mTorr, and it was *in situ* postannealed for 1 h at 450 °C in 1 atm of oxygen atmosphere. As shown in Fig. 1(c), ceramic targets of two end compounds were ablated alternately and the speed of a moving mask was controlled so as to synchronize one period of reflection high-energy electron-diffraction oscillation. Consequently, the $La_{0.6}Sr_{0.4}$ (or $Pr_{0.6}Ca_{0.4}$) content was changed linearly from 0 to 1 over a distance of 8 mm.[7,8] The composition profile of the film was characterized with a scanning electron microscope equipped with an energy dispersive x-ray (EDX) spectrometer.[9] Upper panel of Fig. 1(d) shows the integrated intensity of EDX spectra of Ca normalized by that of Mn. Although the quantitative characterization was difficult due to the interference of strong signal from substrate, the linear change in the Ca content confirms the designed composition spread in the film.

The film used in our experiment has the symmetry close to *Pbnm* space group at room temperature. We found that the [110] axis in the *Pbnm* setting is aligned parallel to the [100] axis in the cubic setting of the substrate. In the following, the pseudocubic setting with the axes corresponding to the substrate is used to denote the crystal axes. In the pseudocubic setting, the film is twin free; as shown in Fig. 1(e), the only single diffraction peak from the film (F) is observed at the position of (0 3 1) and (0 1 3) directions. From the relationship with the diffraction peak from the substrate (S), the lattice constants are estimated [Fig. 3(d)]. As shown in the lower panel of Fig. 1(d), the out-of-plane interplaner spacing

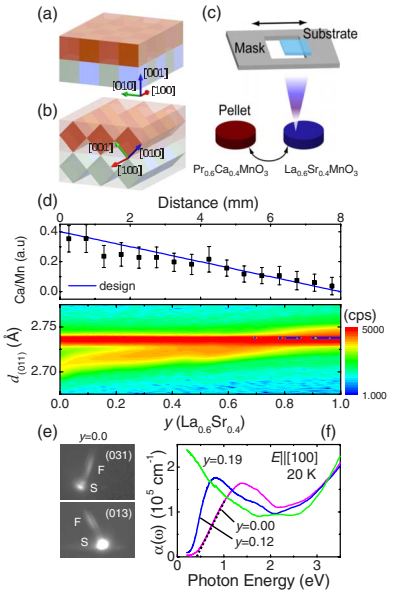

FIG. 1. (Color online) [(a) and (b)] Schematic of the thin films grown on the substrates with surfaces oriented along (001) and (011) directions, respectively. (c) The growth scheme of the composition-spread thin film. (d) Compositional and structural (lower) characteristics of the $(Pr_{0.6}Ca_{0.4})_{1-y}(La_{0.6}Sr_{0.4})_yMnO_3$ film. Upper panel: the ratio of the Ca and Mn compositions shows an almost linear variation with the lateral distance of the film. Lower panel: intensity distribution related to the lattice constant along the surface-normal direction at the room temperature is obtained from concurrent $2\theta/\theta$ x-ray diffraction. The contribution from the substrate is also included showing no change with y. (e) X-ray diffraction peaks of the F and the S at the positions of (0 3 1) and (0 1 3) directions. (f) Absorption coefficient spectra at 20 K for three representative compositions.

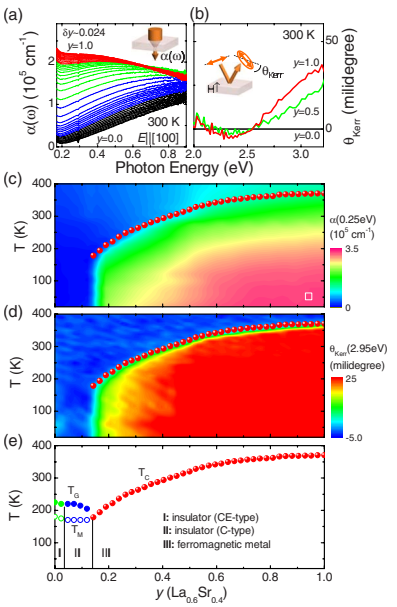

FIG. 2. (Color online) (a) Absorption coefficient spectra at 300 K for different sample compositions. (b) Kerr-rotation angle spectra at 300 K for two representative compositions with the result for y =0.0 as a reference. [(c) and (d)] Contour plots of absorption coefficient at 0.25 eV and Kerr-rotation angle at 2.95 eV in the parameter space of the composition and the temperature. Composition-dependent transition temperatures are indicated in both. The square at the right-bottom corner in (c) indicates a typical unit of the experimental data corresponding to the temperature step of 20 K and the composition step of 0.024. The whole T-y plane is densely covered by the tiling of these units, rendering the extrapolation procedure least ambiguous. (e) Phase diagram of $(Pr_{0.6}Ca_{0.4})_{1-y}(La_{0.6}Sr_{0.4})_yMnO_3$ constructed from the spectroscopic investigations.

$(d_{(011)})$ shows a monotonous increase with increasing the content of the larger size ion, i.e., $La_{0.6}Sr_{0.4}$. In the following, the chemical composition is assumed to change linearly with the lateral position.

As noncontact local probes, various microscopic techniques have been exploited. Optical responses in the mid-infrared and near-infrared/visible region have been obtained using Fourier transform and grating-type spectrometers, respectively. In particular, the equipped microscopes enabled the local probe with a typical spatial resolution of 200 μm which corresponds to the chemical resolution (δy) of ~0.024. The absorption coefficient $\alpha(\omega)$ was estimated from the transmittance $T(\omega)$ as $\alpha(\omega)=-1/t \ln T(\omega)$, where t is the thickness of the film (~40 nm). Sensitive measurement of the Kerr-rotation angle was made via the fast modulation of the polarization status of light using a photoelastic modulator.[10,11] The crossed-Nicols image was taken using a charge coupled device camera under the application of magnetic field with a superconducting magnet. The x-ray $2\theta/\theta$ profile was obtained by moving a sample stage at 200 μm intervals with the narrowed beam down to 200 μm wide with a slit and the diffracted x ray was detected with a scintillation counter. X-ray diffraction measurements using synchrotron radiation at the Photon Factory, KEK, Japan were performed with four-circle diffractometers equipped at Beamline 3A and 4C. The photon energy used was 9.5 keV. The focused beam size is 300 μm along the lateral direction.

Figure 1(f) shows absorption coefficient spectra $\alpha(\omega)$ polarized along the [100] direction at 20 K for three different compositions. For y=0.0, the spectrum shows a clear optical gap formed by an absorption tail of the excitation around 1.5 eV. For y=0.12, the gap becomes smaller, but remains finite as well in the insulating ground state. For y=0.19, the gap is closed and a strong infrared response appears, indicating the metallic nature. Since the filling condition of the conduction band is kept at the same level, such a difference should originate from the change in the conduction bandwidth controlled by the composition (y) variation.

As seen above, the optical response in the mid-infrared region can show distinct behaviors depending on the metal/insulator ground states. In Fig. 2(a), we show $\alpha(\omega)$ in the energy range of 0.18–0.9 eV obtained at 300 K for continuously varying composition with a fine step (δy) of about 0.024. The absorption increases gradually with y, suggesting the increasing metallicity. In Fig. 2(c), we present a contour plot of $\alpha(0.25$ eV) in the plane of temperature (T) and y where a clear distinction can be resolved between the metallic and insulating states.

We examined magnetic states by monitoring the Kerr-rotation angle (θ_{Kerr}),[12] the rotation of the polarization axis

of light upon reflection with a magnetic field ($\mu_0 H \sim 0.2$ T) applied along the surface-normal direction [see the inset of Fig. 2(b)]. To remove the background contribution from the substrate, the result for the $y=0.0$ composition at 300 K, which is in the paramagnetic state, was used as a reference and subtracted from all the other results. As shown in Fig. 2(b), the $y=1.0$ composition exhibits a structured response above 2.5 eV in good agreement with the previous result of the same compound in the ferromagnetic state.[13] Figure 2(d) shows the contour plot of θ_{Kerr} at 2.95 eV, which signifies the temperature- and composition-dependent transition to the ferromagnetic state.

Based on these results, the electronic phase diagram is constructed as shown in Fig. 2(e). (Insulating states will be discussed in detail below.) Both the metallic and ferromagnetic states arise simultaneously, which agrees well with the double-exchange mechanism, i.e., the ferromagnetic arrangement of local spins mediated by itinerant electrons.[14] It is worth to note that the phase evolutions look similar with the case of the bulk counterparts;[6,14,15] the transition temperature to the ferromagnetic/metallic state reaches maximally about 370 K for $y=1.0$ and decreases down to about 200 K for $y \sim 0.14$. In particular, there appears a well-defined vertical phase boundary around $y \sim 0.14$ distinguishing the ferromagnetic/metallic state from the nonferromagnetic/insulating state.

Notwithstanding the similarity of the overall phase evolutions to those for the bulk materials, the behaviors in the insulating side turn out to be distinct. To retrieve useful information about the insulating state, additional analyses were performed on the optical responses. First, we estimated the optical gap E_{gap} for the polarization along the [100] axis by linearly extrapolating the absorption edge to find the crossing point at the zero absorption level, as exemplified by a dotted line in Fig. 1(f). The contour plot for E_{gap} displayed in Fig. 3(a) shows a clear distinction between metallic and insulating states as in the $\alpha(0.25$ eV) map shown in Fig. 2(c), and the onset temperature (T_G) of the increase in the gap size is indicated as a function of y together with the other magnetic transition temperatures (T_M) which were taken from the spectral-weight analysis (not shown). Next, we monitored the optical anisotropy between the polarization along the [100] and [01$\bar{1}$] directions. As shown in Fig. 4(a), the compositional regions in the insulating state, e.g., $y=0.0$ and 0.07, show conspicuous optical anisotropies in the broad spectral range; their optical anisotropies with respect to the light polarization are opposite. For more details, we estimated ΔSW_{nor}, a difference in the spectral weights (SW) from 0.2 to 0.9 eV between polarizations along [100] and [01$\bar{1}$] directions normalized by their sum. Since the optical-region charge dynamics as measured by SW can be strongly anisotropic in the charge/orbital-ordered states depending on their ordering patterns, ΔSW_{nor} can give a good insight into the electronic order of the insulating state.[16] As shown in Fig. 3(b), ΔSW_{nor} for $0.04<y<0.14$ is much larger than in the other regions. Such a composition-dependent anisotropic response is also discerned by the crossed-Nicols image taken in the visible region [Fig. 3(c)]; while the sample shows a homogeneously dark image at 300 K, it shows a strong contrast at 20 K just like the result in the mid-infrared region shown in Fig. 3(b). These observations strongly suggest that two different ground states emerge in the insulating side.

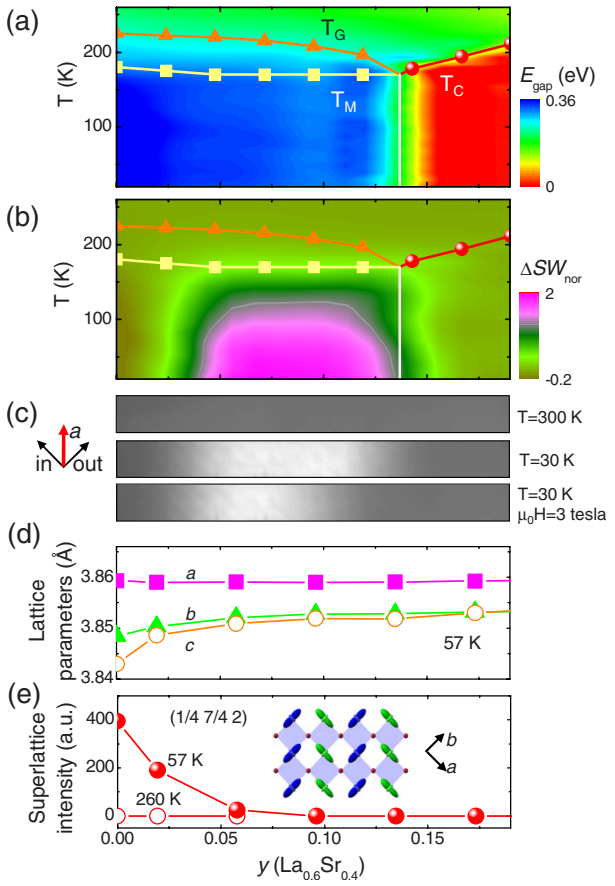

FIG. 3. (Color online) [(a) and (b)] Contour plots of the charge gap and the optical anisotropy, respectively. (c) Visible polarized microscope image obtained in a crossed-Nicols configuration ($\lambda=730$ nm). [(d) and (e)] Composition dependences of the lattice parameters and the integrated intensities of superlattice reflection (1/4 7/4 2). The inset shows the zigzag-type order of $3x^2-r^2$ and $3y^2-r^2$ orbitals which is related to the superlattice reflection.

For the detailed understanding of the insulating states, structural properties have been investigated in terms of the x-ray diffraction. Figure 3(e) shows the compositio dependence of the superlattice reflection around (1/4 7/4 2) which appears at low temperatures, e.g., at 57 K for $y<0.04$. This superlattice reflection has been consistently observed for $Pr_{0.6}Ca_{0.4}MnO_3$ in bulk single-crystal form and can be related to the zigzag-type orbital order as shown in Figs. 3(e) and 4(b).[4,17–19] With this charge/orbital-ordered pattern in the half-doped state as a backbone, additional electrons introduced for this $(Pr_{0.6}Ca_{0.4})_{1-y}(La_{0.6}Sr_{0.4})_yMnO_3$ system tend to occupy $3z^2-r^2$ orbital which will favor the transfer integral of the electron along the c axis. This is actually confirmed by the smaller size of the optical gap with the light E vector along [01$\bar{1}$] than along [100] [Fig. 4(a)].[20,21]

For $0.04<y<0.14$, the compounds do not allow the superlattice reflection at (1/4 7/4 2). Instead, they show much stronger optical anisotropies with the highly asymmetric spectral shape along the [100] direction [see Figs. 1(f) and

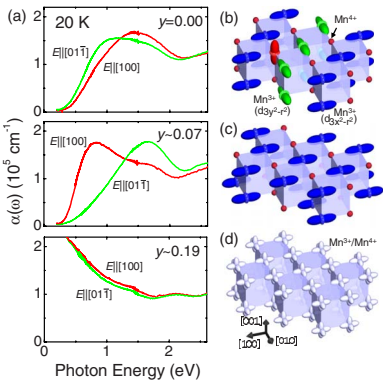

FIG. 4. (Color online) (a) Absorption coefficient spectra at 20 K for three representative compositions using different polarization states of light. [(b), (c), and (d)] Charge-/orbital-ordered states for $y<0.04$, $0.04<y<0.14$, and $0.14<y$, respectively. While the metallic state corresponds to the charge/orbital quantum-disordered state, the insulating states are with a zigzag-type orbital order for $y<0.04$ and a plausibly one-dimensional orbital order for $0.04<y<0.14$ where the charge degree of freedom is supposed to be disordered or short-range ordered. Here, the perfect ionic picture is assumed.

4(a)]. Such a spectral feature for the charge-gap transition is typical of one-dimensional electronic system.[16,22] Tetragonal symmetry with the longest a-axis lattice parameter [Fig. 3(d)] suggests the anisotropic crystal field acting on the Mn site. Such a strain field may host a ground state with one-dimensional orbital order with an orbital shape of $3x^2-r^2$, as shown in Fig. 4(c), which can reasonably explain the optical anisotropy.

The ground states for $(Pr_{0.6}Ca_{0.4})_{1-y}(La_{0.6}Sr_{0.4})_yMnO_3$ thin film are summarized in the phase diagram shown in Fig. 2(e). In the corresponding bulk materials, the CE-type insulating ground state evolves directly into the ferromagnetic/metallic state forming the bicritical phase boundary between them.[6,14,15] In the present case, however, these two states are intervened by the additional insulating state plausibly with one-dimensional $(3x^2-r^2)$ orbital order and C-type spin order. While the entire film is subject to the uniaxial strain as shown in Fig. 3(d), its effect will be amplified near the bicritical phase boundary where competing orders of spin/charge/orbital degrees of freedom are in subtle balance.

Such a phase competition can enhance the response of the electronic state to the external magnetic field. As shown in the crossed-Nicols image at 3 T [Fig. 3(c)], while the phase boundary between two insulating states is robust against the magnetic field, the other phase boundary shifts to the left side. This clearly demonstrates that the insulating state in the intermediate region undergoes a transition to the ferromagnetic/metallic state with the relatively low magnetic field, e.g., ~1 T.

In summary, we exploited various microspectroscopic techniques to investigate the phase evolution in the bandwidth-controlled $(Pr_{0.6}Ca_{0.4})_{1-y}(La_{0.6}Sr_{0.4})_yMnO_3$ system prepared as a composition-spread thin film grown on the anisotropic surface of the substrate. We have demonstrated plentiful phase evolutions between the insulating and the metallic states, and a possibly one-dimensional orbital-ordered state near the critical metal-insulator phase boundary which could be disturbed with a relatively low magnetic field. These results manifest competing electronic orders in manganite thin films that are subject to the anisotropic strain. Further study along this direction will help to realize active devices exploiting the direct phase control based on the correlated electron system in a thin-film form.

We thank H. Nakao for the experimental support and fruitful discussion on the x-ray study. This work was in part supported by Grant-in-Aids for Scientific Research (Grants No. 16076205, No. 20340086, and No. 21760032) from the Ministry of Education, Culture, Sports and Technology (MEXT), Japan, and also by the Japan Society for the Promotion of Science (JSPS) through its Funding Program for World-Leading Innovative R&D on Science and Technology (FIRST Program).

*jslee@ap.t.u-tokyo.ac.jp

[1] C. B. Eom *et al.*, Science **258**, 1766 (1992).
[2] M. Nakamura *et al.*, Appl. Phys. Lett. **86**, 182504 (2005).
[3] Y. Ogimoto *et al.*, Phys. Rev. B **71**, 060403(R) (2005).
[4] Y. Wakabayashi *et al.*, J. Phys. Soc. Jpn. **77**, 014712 (2008).
[5] L. M. Rodriguez-Martinez and J. P. Attfield, Phys. Rev. B **54**, R15622 (1996).
[6] Y. Tomioka and Y. Tokura, Phys. Rev. B **70**, 014432 (2004).
[7] T. Fukumura *et al.*, Appl. Phys. Lett. **77**, 3426 (2000).
[8] H. Koinuma and I. Takeuchi, Nature Mater. **3**, 429 (2004).
[9] T. Fukumura *et al.*, Appl. Surf. Sci. **189**, 339 (2002).
[10] N. Hosaka *et al.*, Appl. Phys. Express **1**, 113001 (2008).
[11] K. Sato, Jpn. J. Appl. Phys. **20**, 2403 (1981).
[12] S. A. McGill *et al.*, Phys. Rev. B **71**, 075117 (2005).
[13] T. Ogasawara *et al.*, Phys. Rev. B **68**, 180407 (2003).
[14] Y. Tokura, Rep. Prog. Phys. **69**, 797 (2006).
[15] Y. Tomioka and Y. Tokura, Phys. Rev. B **66**, 104416 (2002).
[16] K. Tobe *et al.*, Phys. Rev. B **69**, 014407 (2004).
[17] D. Okuyama *et al.*, Appl. Phys. Lett. **95**, 152502 (2009).
[18] Z. Jirak *et al.*, J. Magn. Magn. Mater. **53**, 153 (1985).
[19] While the simple ionic picture is assumed here for a schematic description, it should be noted that the charge disproportionation in the charge-ordered state of manganites deviates from the ionic order, and it is, for example, around 22% for $Pr_{0.5}Ca_{0.5}MnO_3$. Refer to D. Okuyama, Y. Tokunaga, R. Kumai, Y. Taguchi, T. Arima, and Y. Tokura, Phys. Rev. B **80**, 064402 (2009).
[20] Y. Okimoto *et al.*, Phys. Rev. B **57**, R9377 (1998).
[21] S. Grenier *et al.*, Phys. Rev. B **69**, 134419 (2004).
[22] Y. S. Lee *et al.*, Phys. Rev. B **75**, 144407 (2007).